

A node-based smoothed finite element method (NS-FEM) for upper bound solutions to solid mechanics problems

G.R. Liu^{a,b}, T. Nguyen-Thoi^{a,*}, H. Nguyen-Xuan^b, K.Y. Lam^c

^aCenter for Advanced Computations in Engineering Science (ACES), Department of Mechanical Engineering, National University of Singapore, 9 Engineering Drive 1, Singapore 117576, Singapore

^bSingapore-MIT Alliance (SMA), E4-04-10, 4 Engineering Drive 3, Singapore 117576, Singapore

^cSchool of Mechanical and Aerospace Engineering, Nanyang Technological University, 50 Nanyang Avenue, Singapore 639798, Singapore

ARTICLE INFO

Article history:

Received 17 November 2007

Accepted 22 September 2008

Available online 7 November 2008

Keywords:

Finite element method (FEM)

Smoothed finite element method (SFEM)

Upper bound

Lower bound

Global error

Polygonal

ABSTRACT

This paper presents a node-based smoothed finite element method (NS-FEM) for upper bound solutions to solid mechanics problems using a mesh of polygonal elements. The calculation of the system stiffness matrix is performed using strain smoothing technique over the smoothing cells associated with nodes, which leads to line integrations along the edges of the smoothing cells. The numerical results demonstrated that the NS-FEM possesses the following properties: (1) upper bound in the strain energy of the exact solution when a reasonably fine mesh is used; (2) well immune from the volumetric locking; (3) can use polygonal elements with an arbitrary number of sides; (4) insensitive to element distortion.

© 2008 Elsevier Ltd. All rights reserved.

1. Introduction

In order to determine the error in numerical solutions of complicated problems without knowing the exact solution, it is practical to use two numerical models: one gives a lower bound and the other gives an upper bound of the solution. The most popular models giving a lower bound in term of strain energy are the fully-compatible displacement finite element method (FEM) models, which are widely used in solving complicated engineering problems. The model that gives an upper bound can be one of the following models: the stress equilibrium FEM model [1], the recovery of a statically admissible stress field from displacement FEM model [2–4], the hybrid equilibrium FEM model [5,6], the element-based smoothed finite element method (SFEM) model [7,8], the α FEM models [9,10], and the recently proposed LC-PIM model [11]. In the so-called dual analysis in the FEM [1,12,13], a displacement FEM model is usually combined with an equilibrium FEM model. However, such a dual analysis procedure is not popular due to some disadvantages referred to equilibrium models: (1) the equilibrium approach is mathematically complex and hence difficult to implement and more expensive computationally; (2) spurious modes often occur due to the simple fact that tractions cannot be equilibrated by the stress approximation field. Due to these draw-

backs of the equilibrium FEM models, the estimation of the global error based on the dual analysis is not widely used in practical applications to complicated engineering problems.

In the other front of development, a conforming nodal integration technique has been proposed by Chen et al. [14] to stabilize the solutions in the context of the meshfree method and then applied in the natural element method [15]. Liu et al. have applied this technique to formulate the linear conforming point interpolation method (LC-PIM) [16], the linearly conforming radial point interpolation method (LC-RPIM) [17] and the element-based smoothed finite element method (SFEM) [8,18]. Liu and Zhang [11] have provided an intuitive explanation and showed numerically that when a reasonably fine mesh is used, the LC-PIM has an upper bound property in the strain energy. The same finding is obtained for LC-RPIM, meaning that the LC-RPIM also has the similar upper bound property [17]. A more detailed theoretical study on a generalized smoothing technique and the smoothed Galerkin formulations has been conducted with intensive examination on the properties of the smoothed bi-linear forms and the smoothed Galerkin solutions [31].

In order to make use of the upper bound property of the LC-PIM and LC-RPIM from the meshfree context into the FEM framework and to overcome the above disadvantages of the equilibrium FEM models, this paper proposes a node-based smoothed finite element method (NS-FEM) for upper bound solutions to solid mechanics problems. The calculation of the system stiffness matrix is

* Corresponding author. Tel.: +65 9860 4962.

E-mail address: g0500347@nus.edu.sg (T. Nguyen-Thoi).

performed using strain smoothing technique over the cells associated with nodes, which leads to line integrations along the edges of the smoothing cells and such an integration can be evaluated using the interpolated shape function (not their derivatives). The numerical results demonstrated that the NS-FEM possesses the following properties: (1) when a reasonably fine mesh is used, it gives upper bound (in the case of homogeneous essential boundary conditions) in the strain energy of the exact solution; (2) it is well immune from the volumetric locking; (3) it allows the use of polygonal elements with an arbitrary number of sides. One other important advantage of the NS-FEM is that due to the use of the smoothed strain, the domain integration on the cell becomes line integration along the boundary of the cell, and the field gradients are computed directly using only the shape functions themselves and no explicit analytical form of shape functions is required. As a result, no mapping or coordinate transformation is involved in the NS-FEM and its element is allowed to be of arbitrary shape. The problem domain can be discretized in more flexible ways, and even severely distorted elements can be used.

The NS-FEM can be viewed as a variant model of FEM, but the shape functions used in NS-FEM are in general different from those in FEM. In NS-FEM, we do not construct shape functions explicitly, instead we simply perform point interpolation using nodes within the element that host the point of interest. The NS-FEM has very attractive properties that are complementary to the FEM. It can be applied easily to 4-node quadrilateral or triangular elements without any modification in the formulation and procedures. When only triangular elements are used, the NS-FEM produces the same results as the method NIFEM proposed by Dohrmann et al. [19] or to the LC-PIM using linear interpolation [20]. The NS-FEM is more general than the NIFEM. For 2D problems, the NS-FEM formulation can be applied for triangular, quadrilateral and n -sided polygonal elements of any order, where the compatible strain field is not generally constant. The NIFEM formulation [19] is applicable only to uniform strain elements, and hence it can be only applied to linear triangular/tetrahedron elements. In addition, the numerical procedure of the NS-FEM and the NIFEM are also different. The NS-FEM uses the value of shape function at points and the integration of the weak form is performed along the boundary of the smoothing cell associated with nodes, while the NIFEM uses the derivative of shape functions and the integration of the weak form is based on the whole domain of the cell. Hence, the NIFEM can be viewed as a special case of the NS-FEM. Note also that, the NS-FEM is evolved from the SFEM [8,18] in which the strain smoothing technique was applied based on elements, and they all have the same features of strain smoothing operation.

The NS-FEM is different from the LC-PIM in the following ways. The LC-PIM was basically conceived from the meshfree procedures: shape functions are constructed using nodes beyond the cells/elements, and they can be linear, quadratic or even higher order depending on the number of nodes used in the support domain. In the case of LC-RPIM [17], the selection of nodes can practically be entirely free, and the consistency of the shape functions can be arbitrarily high. The foundation of the LC-PIM is based on the generalized smoothed gradient smoothing technique [31]. Therefore, the NS-FEM can be considered as a special case of the LC-PIM.

A simple and practical procedure is proposed to determine both the upper and lower bounds in the strain energy, by combining the NS-FEM with the standard FEM (for triangular and quadrilateral elements) or with the element-based smoothed FEM (SFEM) (for the n -sided polygonal elements) [18]. Such bounds are obtained using only one set of mesh and without knowing the exact solution of the problem that can be very complicated as long as a standard FEM model can be built.

The paper is outlined as follows. In Section 2, the idea of the NS-FEM is introduced. In Section 3, the variational basis of the NS-FEM is presented. Construction of the NS-FEM shape function is described in Section 4. In Section 5, the upper bound property of the NS-FEM is presented briefly and numerical implementation issues are discussed in Section 6. Some numerical examples are analyzed in Section 7 and some concluding remarks are made in Section 8.

2. The idea of the NS-FEM

2.1. Briefing on the finite element method (FEM) [21–23]

The discrete equations of the FEM are generated from the Galerkin weak form and the integration is performed on the basis of element as follows:

$$\int_{\Omega} (\nabla_s \delta \mathbf{u})^T \mathbf{D} (\nabla_s \mathbf{u}) d\Omega - \int_{\Omega} \delta \mathbf{u}^T \mathbf{b} d\Omega - \int_{\Gamma_t} \delta \mathbf{u}^T \bar{\mathbf{t}} d\Gamma = 0, \quad (1)$$

where \mathbf{b} is the vector of external body forces, \mathbf{D} is a symmetric positive definite (SPD) matrix of material constants, $\bar{\mathbf{t}}$ is the prescribed traction vector on the natural boundary Γ_t , \mathbf{u} is trial functions, $\delta \mathbf{u}$ is test functions and $\nabla_s \mathbf{u}$ is the symmetric gradient of the displacement field.

The FEM uses the following trial and test functions:

$$\mathbf{u}^h(\mathbf{x}) = \sum_{I=1}^{NP} \mathbf{N}_I(\mathbf{x}) \mathbf{d}_I; \quad \delta \mathbf{u}^h(\mathbf{x}) = \sum_{I=1}^{NP} \mathbf{N}_I(\mathbf{x}) \delta \mathbf{d}_I, \quad (2)$$

where NP is the number of the nodal variables of the element, \mathbf{d}_I is the nodal displacement vector and $\mathbf{N}_I(\mathbf{x})$ is the shape function matrix.

By substituting the approximations, \mathbf{u}^h and $\delta \mathbf{u}^h$, into the weak form and invoking the arbitrariness of virtual nodal displacements, Eq. (1) yields the standard discretized algebraic system equation:

$$\mathbf{K}^{\text{FEM}} \mathbf{d} = \mathbf{f}, \quad (3)$$

where \mathbf{K}^{FEM} is the stiffness matrix, \mathbf{f} is the element force vector, that are assembled with entries of

$$\mathbf{K}_{IJ}^{\text{FEM}} = \int_{\Omega} \mathbf{B}_I^T \mathbf{D} \mathbf{B}_J d\Omega, \quad (4)$$

$$\mathbf{f}_I = \int_{\Omega} \mathbf{N}_I^T(\mathbf{x}) \mathbf{b} d\Omega + \int_{\Gamma_t} \mathbf{N}_I^T(\mathbf{x}) \bar{\mathbf{t}} d\Gamma \quad (5)$$

with the *strain matrix* defined as

$$\mathbf{B}_I(\mathbf{x}) = \nabla_s \mathbf{N}_I(\mathbf{x}). \quad (6)$$

2.2. The NS-FEM for n -sided polygonal elements

In the NS-FEM, the domain discretization is still based on polygonal elements of arbitrary number of sides, but the integration required in the weak form (1) is performed based on the nodes, and strain smoothing technique [14] is used. In such a nodal integration process, the problem domain Ω is divided into smoothing cells associated with nodes such that $\Omega = \sum_{k=1}^{N_n} \Omega^{(k)}$ and $\Omega^{(i)} \cap \Omega^{(j)} = \emptyset$, $i \neq j$, in which N_n is the total number of field nodes located in the entire problem domain. For n -sided polygonal elements, the cell $\Omega^{(k)}$ associated with the node k is created by connecting sequentially the mid-edge-point to the central points of the surrounding n -sided polygonal elements of the node k as shown in Fig. 1. As a result, each n -sided polygonal element will be divided into n four-side sub-domains and each sub-domain is attached with the nearest field node. The cell associated with the node k is then created by combination of each nearest sub-domain of all elements around the node k .

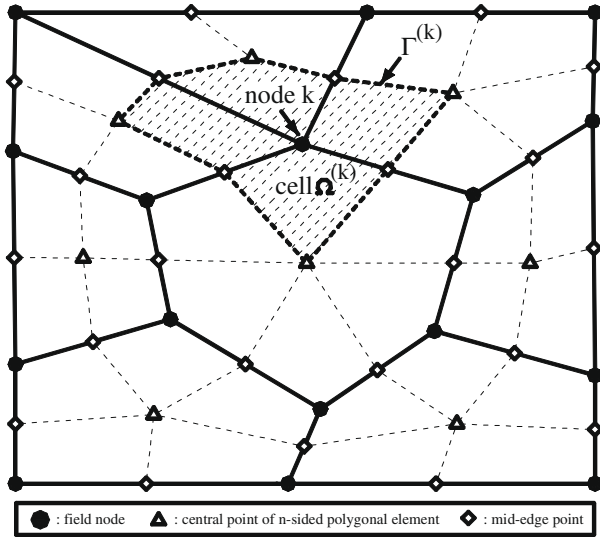


Fig. 1. n -Sided polygonal elements and the smoothing cells associated with nodes.

Introducing the node-based smoothing operation, the strain $\boldsymbol{\varepsilon} = \nabla_s \mathbf{u}$ used in Eq. (1) is assumed to be the *smoothed* strain on the cell $\Omega^{(k)}$ associated with node k :

$$\tilde{\boldsymbol{\varepsilon}}_k = \int_{\Omega^{(k)}} \boldsymbol{\varepsilon}(\mathbf{x}) \Phi_k(\mathbf{x}) d\Omega = \int_{\Omega^{(k)}} \nabla_s \mathbf{u}(\mathbf{x}) \Phi_k(\mathbf{x}) d\Omega, \quad (7)$$

where $\Phi_k(\mathbf{x})$ is a given smoothing function that satisfies at least unity property

$$\int_{\Omega^{(k)}} \Phi_k(\mathbf{x}) d\Omega = 1. \quad (8)$$

Using the following constant smoothing function:

$$\Phi_k(\mathbf{x}) = \begin{cases} 1/A^{(k)}, & \mathbf{x} \in \Omega^{(k)}, \\ 0, & \mathbf{x} \notin \Omega^{(k)}, \end{cases} \quad (9)$$

where $A^{(k)} = \int_{\Omega^{(k)}} d\Omega$ is the area of the cell $\Omega^{(k)}$ and applying the divergence theorem, one can obtain the smoothed strain that is constant over the domain $\Omega^{(k)}$

$$\tilde{\boldsymbol{\varepsilon}}_k = \frac{1}{A^{(k)}} \int_{\Gamma^{(k)}} \mathbf{n}^{(k)}(\mathbf{x}) \mathbf{u}(\mathbf{x}) d\Gamma, \quad (10)$$

where $\Gamma^{(k)}$ is the boundary of the domain $\Omega^{(k)}$ as shown in Fig. 1, and $\mathbf{n}^{(k)}(\mathbf{x})$ is the outward normal vector matrix on the boundary $\Gamma^{(k)}$ and has the following form for 2D problems:

$$\mathbf{n}^{(k)}(\mathbf{x}) = \begin{bmatrix} n_x^{(k)} & 0 \\ 0 & n_y^{(k)} \\ n_y^{(k)} & n_x^{(k)} \end{bmatrix}. \quad (11)$$

In the NS-FEM, the trial function $\mathbf{u}^h(\mathbf{x})$ is the same as in Eq. (2) of the FEM and therefore, the force vector \mathbf{f} in the NS-FEM is calculated in the same way as in the FEM.

Substituting Eq. (2) into Eq. (10), the smoothed strain on the cell $\Omega^{(k)}$ associated with node k can be written in the following matrix form of nodal displacements:

$$\tilde{\boldsymbol{\varepsilon}}_k = \sum_{I \in N^{(k)}} \tilde{\mathbf{B}}_I(\mathbf{x}_k) \mathbf{d}_I, \quad (12)$$

where $N^{(k)}$ is the number of nodes that are directly connected to node k and $\tilde{\mathbf{B}}_I(\mathbf{x}_k)$ is termed as the smoothed strain matrix on the cell $\Omega^{(k)}$

$$\tilde{\mathbf{B}}_I(\mathbf{x}_k) = \begin{bmatrix} \tilde{b}_{Ix}(\mathbf{x}_k) & 0 \\ 0 & \tilde{b}_{Iy}(\mathbf{x}_k) \\ \tilde{b}_{Iy}(\mathbf{x}_k) & \tilde{b}_{Ix}(\mathbf{x}_k) \end{bmatrix} \quad (13)$$

and it is calculated numerically using

$$\tilde{b}_{Ih}(\mathbf{x}_k) = \frac{1}{A^{(k)}} \int_{\Gamma^{(k)}} n_h^{(k)}(\mathbf{x}) N_I(\mathbf{x}) d\Gamma \quad (h = x, y). \quad (14)$$

When a linear compatible displacement field along the boundary $\Gamma^{(k)}$ is used, one Gaussian point is sufficient for line integration along each segment of boundary $\Gamma_i^{(k)}$ of $\Omega^{(k)}$, the above equation can be further simplified to its algebraic form

$$\tilde{b}_{Ih}(\mathbf{x}_k) = \frac{1}{A^{(k)}} \sum_{i=1}^M n_{ih}^{(k)} N_I(\mathbf{x}_i^{\text{GP}}) l_i^{(k)} \quad (h = x, y), \quad (15)$$

where M is the total number of the boundary segments of $\Gamma_i^{(k)}$, \mathbf{x}_i^{GP} is the midpoint (Gaussian point) of the boundary segment of $\Gamma_i^{(k)}$, whose length and outward unit normal are denoted as $l_i^{(k)}$ and $n_{ih}^{(k)}$, respectively.

Eq. (15) implies that in the NS-FEM, only shape function values at some particular points along segments of boundary $\Gamma_i^{(k)}$ are needed and no explicit analytical form is required. This gives tremendous freedom in shape function construction which will be presented in Section 4.

In particular for triangular elements, the smoothed strain matrix $\tilde{\mathbf{B}}_I(\mathbf{x}_k)$ can be assembled by other way

$$\tilde{\mathbf{B}}_I(\mathbf{x}_k) = \frac{1}{A^{(k)}} \sum_{j=1}^{N_e^{(k)}} \frac{1}{3} A_e^{(j)} \mathbf{B}_j \quad (16)$$

where $N_e^{(k)}$ is the number of elements around the node k , $A_e^{(j)}$ and \mathbf{B}_j are the area and the strain gradient matrix of the j th element around the node k , respectively, and $A^{(k)}$ is calculated specifically by

$$A^{(k)} = \int_{\Omega^{(k)}} d\Omega = \frac{1}{3} \sum_{j=1}^{N_e^{(k)}} A_e^{(j)} \quad (17)$$

Note that with this formulation, only the area and the usual “compatible” strain matrices \mathbf{B}_j by Eq. (6) of triangular elements are needed to calculate the system stiffness matrix for the NS-FEM. This formulation is quite straightforward to extend the NS-FEM for the 3D problems using tetrahedral elements in which the smoothed strain matrix $\tilde{\mathbf{B}}_I(\mathbf{x}_k)$ is assembled by

$$\tilde{\mathbf{B}}_I(\mathbf{x}_k) = \frac{1}{V^{(k)}} \sum_{j=1}^{N_e^{(k)}} \frac{1}{4} V_e^{(j)} \mathbf{B}_j \quad (18)$$

where $V_e^{(j)}$ and \mathbf{B}_j are the volume and the compatible strain gradient matrix of the j th tetrahedral element around the node k , respectively, and $V^{(k)}$ is calculated specifically by

$$V^{(k)} = \int_{\Omega^{(k)}} d\Omega = \frac{1}{4} \sum_{j=1}^{N_e^{(k)}} V_e^{(j)} \quad (19)$$

The stiffness matrix $\tilde{\mathbf{K}}$ of the system is then assembled by a similar process as in the FEM

$$\tilde{\mathbf{K}}_{IJ} = \sum_{k=1}^{N_n} \tilde{\mathbf{K}}_{IJ}^{(k)}, \quad (20)$$

where $\tilde{\mathbf{K}}_{IJ}^{(k)}$ is the stiffness matrix associated with node k and is calculated by

$$\tilde{\mathbf{K}}_{IJ}^{(k)} = \int_{\Omega^{(k)}} \tilde{\mathbf{B}}_I^T \mathbf{D} \tilde{\mathbf{B}}_J d\Omega = \tilde{\mathbf{B}}_I^T \mathbf{D} \tilde{\mathbf{B}}_J A^{(k)}. \quad (21)$$

It can be seen that the cell element $\Omega^{(k)}$ associated with node k in the NS-FEM possesses the properties of a hybrid finite element: (i) the stress satisfies the equilibrium equation inside the cell domain $\Omega^{(k)}$ because the stress is constant due to smoothed strain; (ii) the displacement field is linear compatible along the boundary $\Gamma^{(k)}$. Property (ii) will be examined in detail through the shape function construction in Section 4.

3. Variational basis of the NS-FEM

Property 1. The NS-FEM is variationally consistent.

Proof. In the NS-FEM, the generalized Galerkin weak form is used with the smoothed strain (7) instead of the compatible strain $\varepsilon = \nabla_s \mathbf{u}$, the variational consistency thus needs to be examined. To this end, we start with the modified Hellinger–Reissner variational principle with the assumed strain vector $\tilde{\varepsilon}$ and displacements \mathbf{u} as independent field variables [24]:

$$U(\mathbf{u}, \tilde{\varepsilon}) = - \int_{\Omega} \frac{1}{2} \tilde{\varepsilon}^T \mathbf{D} \tilde{\varepsilon} d\Omega + \int_{\Omega} (\mathbf{D} \tilde{\varepsilon})^T (\nabla_s \mathbf{u}) d\Omega - \int_{\Omega} \mathbf{u}^T \mathbf{b} d\Omega - \int_{\Gamma_t} \mathbf{u}^T \bar{\mathbf{t}} d\Gamma. \quad (22)$$

Performing the variation using the chain rule, one obtains

$$\begin{aligned} \delta U(\mathbf{u}, \tilde{\varepsilon}) = & - \int_{\Omega} \delta \tilde{\varepsilon}^T \mathbf{D} \tilde{\varepsilon} d\Omega + \int_{\Omega} \delta \tilde{\varepsilon}^T \mathbf{D} (\nabla_s \mathbf{u}) d\Omega + \int_{\Omega} \tilde{\varepsilon}^T \mathbf{D} (\nabla_s \delta \mathbf{u}) d\Omega \\ & - \int_{\Omega} \delta \mathbf{u}^T \mathbf{b} d\Omega - \int_{\Gamma_t} \delta \mathbf{u}^T \bar{\mathbf{t}} d\Gamma = 0. \end{aligned} \quad (23)$$

Substituting the approximations (2), (12) into (23) and using the arbitrary property of variation, we obtain

$$\mathbf{K}^{\text{two-field}} \mathbf{d} = \mathbf{f}, \quad (24)$$

where $\mathbf{K}^{\text{two-field}}$ is the smoothed stiffness matrix given by Eq. (25), and \mathbf{f} is the element force vector given by Eq. (26)

$$\begin{aligned} \mathbf{K}_{ij}^{\text{two-field}} = & - \int_{\Omega} \tilde{\mathbf{B}}_i^T \mathbf{D} \tilde{\mathbf{B}}_j d\Omega + 2 \int_{\Omega} \tilde{\mathbf{B}}_i^T \mathbf{D} \mathbf{B}_j(\mathbf{x}) d\Omega, \\ = & - \sum_{k=1}^{N_n} \int_{\Omega^{(k)}} \tilde{\mathbf{B}}_i^T \mathbf{D} \tilde{\mathbf{B}}_j d\Omega + 2 \sum_{k=1}^{N_n} \int_{\Omega^{(k)}} \tilde{\mathbf{B}}_i^T \mathbf{D} \mathbf{B}_j(\mathbf{x}) d\Omega \end{aligned} \quad (25)$$

$$\mathbf{f}_i = \int_{\Omega} \mathbf{N}_i^T(\mathbf{x}) \mathbf{b} d\Omega + \int_{\Gamma_t} \mathbf{N}_i^T(\mathbf{x}) \bar{\mathbf{t}} d\Gamma. \quad (26)$$

Using smoothed matrices $\tilde{\mathbf{B}}_i$ in Eq. (13), the following orthogonal condition is satisfied [25]:

$$\begin{aligned} \int_{\Omega^{(k)}} \tilde{\mathbf{B}}_i^T \mathbf{D} \mathbf{B}_j(\mathbf{x}) d\Omega = & \tilde{\mathbf{B}}_i^T \mathbf{D} \int_{\Omega^{(k)}} \mathbf{B}_j(\mathbf{x}) d\Omega \\ = & \tilde{\mathbf{B}}_i^T \mathbf{D} A^{(k)} \int_{\Omega^{(k)}} \frac{\mathbf{B}_j(\mathbf{x})}{A^{(k)}} d\Omega = \tilde{\mathbf{B}}_i^T \mathbf{D} \tilde{\mathbf{B}}_j A^{(k)} \\ = & \int_{\Omega^{(k)}} \tilde{\mathbf{B}}_i^T \mathbf{D} \tilde{\mathbf{B}}_j d\Omega \end{aligned} \quad (27)$$

and from Eq. (25) we then have

$$\mathbf{K}_{ij}^{\text{two-field}} = \mathbf{K}_{ij}^{\text{NS-FEM}} = \int_{\Omega} \tilde{\mathbf{B}}_i^T \mathbf{D} \tilde{\mathbf{B}}_j d\Omega = \sum_{k=1}^{N_n} \int_{\Omega^{(k)}} \tilde{\mathbf{B}}_i^T \mathbf{D} \tilde{\mathbf{B}}_j d\Omega. \quad (28)$$

The NS-FEM uses directly Eq. (28) to calculate the stiffness matrix, therefore, the NS-FEM is “variationally consistent”.

4. Construction of the NS-FEM shape function: point interpolation technique

In the NS-FEM, by using the smoothed strain of the cell $\Omega^{(k)}$ associated with the node k , the domain integration becomes line

integration along the boundary $\Gamma^{(k)}$ of the cell. Only the shape function itself at some particular points along segments of boundary is used and no explicit analytical form is required. When a linear compatible displacement field along the boundary $\Gamma^{(k)}$ is used, one Gauss point at midpoint on each edge is sufficient for accurate boundary integration. The values of the shape functions at these Gauss points, e.g., point #a on the edge A–B shown in Fig. 2, are evaluated averagely using two related nodes on the edge: points #A and #B.

In order to construct a linear compatible displacement field along the boundary $\Gamma^{(k)}$ of the cell, the following conditions of the shape functions for the discrete points of an n -sided polygonal element need to be satisfied: (i) delta function: $N_i(\mathbf{x}_j) = \delta_{ij}$; (ii) partition of unity: $\sum_{i=1}^n N_i(\mathbf{x}) = 1$; (iii) linear consistency: $\sum_{i=1}^n N_i(\mathbf{x}) \mathbf{x}_i = \mathbf{x}$; (iv) linear compatibility: linear shape functions along elements sides; (v) linear shape functions along lines connecting the central point and midpoints of sides, e.g., line B–A or line B–C; (vi) values of the shape function for the central points of n -sided polygonal elements, e.g., points #B or #I, are evaluated as

$$\left[\frac{1}{n} \quad \frac{1}{n} \quad \dots \quad \frac{1}{n} \right] \quad (\text{size: } 1 \times n) \quad (29)$$

with the coordinates of the central points calculated simply using

$$x_c = \frac{1}{n} \sum_{i=1}^n x_i, \quad y_c = \frac{1}{n} \sum_{i=1}^n y_i, \quad (30)$$

where the number of nodes n of the polygonal element may be different from one element to the other and x_i, y_i are the coordinates of nodes of the n -sided polygonal element.

The condition (iii) is essential to reproduce the linear polynomial fields such as in the standard patch test. With the condition (iv), the values of the shape functions of the midpoints on the sides of the elements, e.g., points #A on the side 1–2, are the average of those at two related field nodes on the side: points #1 and #2. With conditions (v) and (vi), a linear compatible displacement field along the boundary $\Gamma^{(k)}$ of the cell $\Omega^{(k)}$ associated with the node k is constructed.

With such novel and simple element-based point interpolation technique, any shape function satisfying the six above conditions can be used in the NS-FEM. It should be mentioned that the purpose of introducing the central points and midpoints of sides is to facilitate the evaluation of the shape function at the Gauss

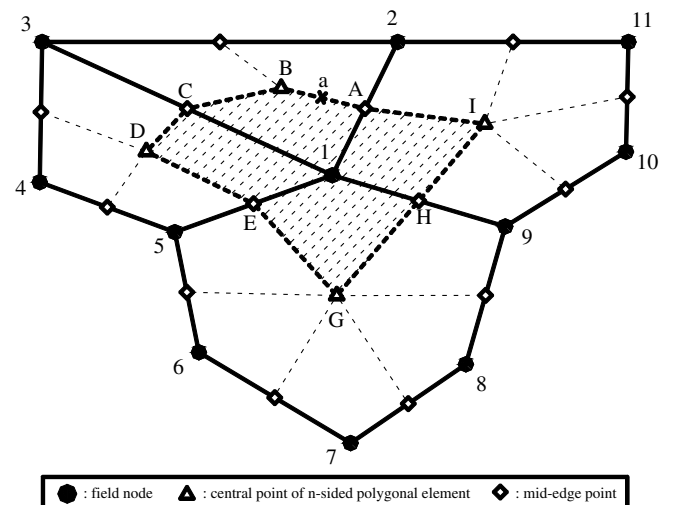


Fig. 2. Construction of simple averaging shape functions for n -sided polygonal elements.

points and to ensure the linear compatible property along the edges of the cell connecting the central point and midpoints of sides. No extra degrees of freedom are associated with these points. In other words, these points carry no additional field variable. This means that the nodal unknowns in the NS-FEM are the same as those in the FEM of the same mesh. The solutions of the unknowns of the NS-FEM and FEM are different.

It is easy to see that the bilinear and linear shape functions for 4-node quadrilateral and triangular elements of the standard FEM satisfy naturally the six above conditions. Hence, the NS-FEM can be applied easily to traditional 4-node quadrilateral or triangular elements without any modification.

Different from the standard isoparametric finite elements, the NS-FEM obtains shape functions without using coordinate transformation or mapping. Hence the field domain can be discretized in a much more flexible way, and even severely distorted elements can be used, as will be shown in the numerical examples. The similar element-based interpolation technique was proposed for SFEM by Dai et al. [18].

5. Upper bound property of the NS-FEM

Property 2. *The numerical results demonstrated that when a reasonably fine mesh is used, the strain energy of numerical solution $E_{\text{NS-FEM}}(\mathbf{d})$ obtained from the NS-FEM solution has the following relationship with the total strain energy of exact solution E_{exact} :*

$$E_{\text{NS-FEM}}(\mathbf{d}) \geq E_{\text{exact}}, \quad (31)$$

where

$$E_{\text{NS-FEM}} = \frac{1}{2} \mathbf{d}^T \mathbf{K}_{\text{NS-FEM}} \mathbf{d}, \quad (32)$$

$$E_{\text{exact}} = \frac{1}{2} \lim_{N_e \rightarrow \infty} \sum_{i=1}^{N_e} \int_{\Omega_i} \boldsymbol{\varepsilon}_i^T \mathbf{D} \boldsymbol{\varepsilon}_i d\Omega. \quad (33)$$

A proof procedure and arguments that shows the same property, Eq. (31), of the LC-PIM can be found in Ref. [11]. In this paper, we focus on the phenomenon from the numerical results rather than the theoretical examination of the phenomenon. An intuitive explanation on why the NS-FEM can always produce upper bound solution may be given as follows. The FEM model underestimates the strain energy by approximating the *continuous* exact strain field by a piecewise-constant strain field over the elements (consistency reduced a little *within* the elements), while the NS-FEM model overestimates the strain energy by approximating the *discontinuous* FEM strain field by a piecewise-constant strain field over the node-based smoothing cells (consistency increased a lot *within* the cells). Therefore, the overestimation will be larger than the underestimation, as long as the mesh used is reasonably fine.

6. Numerical implementation

6.1. Domain discretization with polygonal elements of the Voronoi diagram

The procedure to discretize a problem domain using polygonal elements of the Voronoi diagram can be described as follows [26].

The problem domain and its boundaries are first discretized by a set of properly scattered points $\mathbf{P} := \{p_1, p_2, \dots, p_n\}$. Based on the given points, the domain is further decomposed into the same number of Voronoi cells $\mathbf{C} := \{C_1, C_2, \dots, C_n\}$ according to the nearest-neighbour rule defined by

$$C_i = \{\mathbf{x} \in \mathbb{R}^2 : d(\mathbf{x}, \mathbf{x}_i) < d(\mathbf{x}, \mathbf{x}_j) \quad \forall j \neq i\} \quad \forall i. \quad (34)$$

The shape of these Voronoi cells is generally irregular but they are convex polygons as shown in Fig. 3. The initial point p_i is regarded as the representative point of the i th element. Once we get the information of these Voronoi diagrams, a set of polygonal elements is then formed for our numerical analysis.

The following points need to be noted: (i) the original discrete points \mathbf{P} only serve as numerical devices for domain decomposition and do not function in following numerical analysis; (ii) if we prefer more regular elements, such as rectangular elements, hexagon elements, we need to arrange a special point pattern \mathbf{P} before the generation of Voronoi diagrams; (iii) for demonstration purpose, we arrange the initial points in an arbitrary form in the following numerical examples regardless of the issue of computational cost. As a result, the number of elements sides is generally changing from element to element; (iv) the NS-FEM does not require the elements to be convex (see Section 7.1); (v) triangular and quadrilateral elements used in the FEM can be used directly in the NS-FEM without any alterations.

6.2. Procedure of the NS-FEM

The numerical procedure for the NS-FEM is briefly as follows:

1. Divide the domain into a set of elements and obtain information on nodes coordinates and element connectivity.
2. Determine the area of cells $\Omega^{(k)}$ associated with nodes k and find neighbouring cells of each node.
3. Loop over all the nodes:
 - (a) Determine the node connecting information of cell $\Omega^{(k)}$ associated with node k ;
 - (b) Determine the outward unit normal of each boundary side for cell $\Omega^{(k)}$;
 - (c) Compute the matrix $\tilde{\mathbf{B}}_I(\mathbf{x}_k)$ using Eq. (13);
 - (d) Evaluate the stiffness matrix using Eq. (21) and force vector of the current cell;
 - (e) Assemble the contribution of the current cell to form the system stiffness matrix using Eq. (20) and force vector;
4. Implement essential boundary conditions.
5. Solve the system equations to obtain the nodal displacements.
6. Evaluate strains and stresses at nodes of interest.

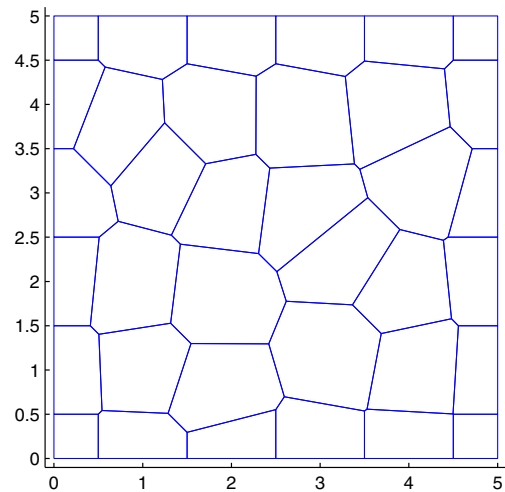


Fig. 3. Voronoi diagram.

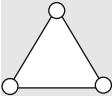
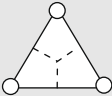
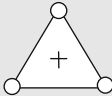
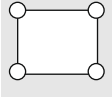
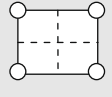
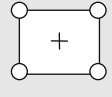
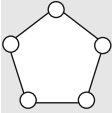
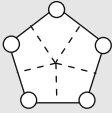
6.3. Rank test for the stiffness matrix

Property 3. The NS-FEM possesses only “legal” zero-energy modes that represents the rigid motions, and there exists no spurious zero-energy mode.

It is known that from the work on the elemental SFEM [8] that an elemental SFEM model can have spurious zero-energy modes when the entire element is used as a smoothing cell. This is because “sampling” smoothing cells are insufficient. In the present node-based SFEM, however, we found that the NS-FEM possesses only “legal” zero-energy modes that represents the rigid motions, and there exists no spurious zero-energy mode. This is ensured by the following key reasons:

- (i) The numerical integration used to evaluate Eq. (28) in the NS-FEM satisfies the necessary condition given in Section 6.1.3 in Ref. [27]. This is true for all possible NS-FEM models, as detailed in Table 1.
- (ii) The nodal strain smoothing operation ensures linearly independent columns (or rows) in the stiffness matrix.
- (iii) The shape functions used in the NS-FEM are of partition of unity. Therefore, no deformed zero-energy mode will appear in the NS-FEM. In other words, any deformation (except the rigid motions) will result in strain energy in an NS-FEM model.

Table 1
Existence of spurious zero-energy modes in an element

Type of element	Nodal-SFEM	FEM with reduced integration
 Triangle $N_R = 3$	 $n_Q = 3, N_Q = 3 \times n_Q = 9$ $n_t = 3, N_u = 2 \times n_t = 6$ $N_Q > N_u - N_R$ \Rightarrow Spurious zero-energy modes not possible	 $n_Q = 1, N_Q = 3 \times n_Q = 3$ $n_t = 3, N_u = 2 \times n_t = 6$ $N_Q = N_u - N_R$ \Rightarrow Spurious zero-energy modes not possible
 Quadrilateral $N_R = 3$	 $n_Q = 4, N_Q = 3 \times n_Q = 12$ $n_t = 4, N_u = 2 \times n_t = 8$ $N_Q > N_u - N_R$ \Rightarrow Spurious zero-energy modes not possible	 $n_Q = 1, N_Q = 3 \times n_Q = 3$ $n_t = 4, N_u = 2 \times n_t = 8$ $N_Q < N_u - N_R$ \Rightarrow Spurious zero-energy modes possible Not applicable
 $(n > 4)$ n-Sided polygonal $N_R = 3$	 $n_t = n, N_u = 2 \times n_t = 2n$ $n_Q = n, N_Q = 3 \times n_Q = 3n$ $N_Q > N_u - N_R$ \Rightarrow Spurious zero-energy modes not possible	 $n_Q = 1, N_Q = 3 \times n_Q = 3$ $n_t = n, N_u = 2 \times n_t = 2n$ $N_Q < N_u - N_R$ \Rightarrow Spurious zero-energy modes possible Not applicable

Note: N_R : number of DOFs of rigid motion.
 n_Q : number of quadrature points/cells.
 N_Q : number of independent equations.
 n_t : number of nodes.
 N_u : number of total DOFs.

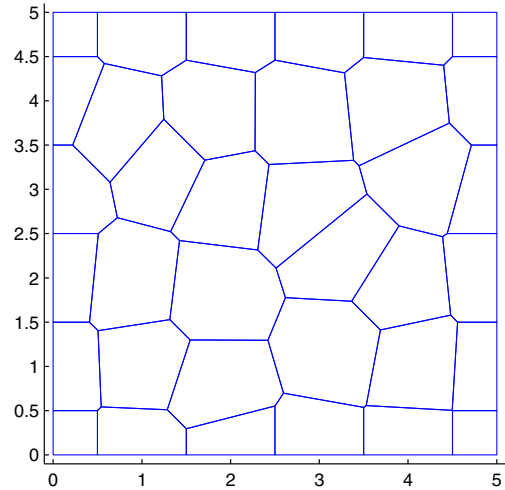


Fig. 4. Domain discretization of a square patch using 36 n -sided polygonal elements.

6.4. Standard patch test

Satisfaction of the standard patch test requires that the displacements of all the interior nodes follow “exactly” (to machine precision) the same linear function of the imposed displacement. A domain discretization of a square patch using 36 n -sided polygonal elements is shown in Fig. 4. The following error norm in displacements is used to examine the computed results:

$$e_d = \frac{\sum_{i=1}^{ndof} |u_i - u_i^h|}{\sum_{i=1}^{ndof} |u_i|} \times 100\%, \quad (35)$$

where u_i is the exact solution, u_i^h is the numerical solution and $ndof$ is the number of degrees of freedom of the system.

The parameters are taken as $E = 100$, $\nu = 0.3$ and the linear displacement field is given by

$$\begin{aligned} u &= x, \\ v &= y. \end{aligned} \quad (36)$$

It is found that the NS-FEM can pass the standard patch test within machine precision with the error norm in displacements: $e_d = 5.22e-13$ (%).

7. Numerical examples

In this section, some examples will be analyzed to demonstrate the properties of the present method. Three kinds of element are used: n -sided polygonal, 4-node quadrilateral and triangular elements. To emphasize the upper bound property of strain energy of the NS-FEM, the results of n -sided polygonal elements of the present method (NS-FEM) will be compared with those of the elemental SFEM with n -sided polygonal (SFEM) [18], while the results of 4-node quadrilateral (NS-FEM-Q4) and triangular elements (NS-FEM-T3) of the present method will be compared with those of the standard displacement FEM (FEM-Q4 and FEM-T3). The error norm of displacement is given in Eq. (35).

7.1. Cantilever loaded at the end

A cantilever with length L and height D is studied as a benchmark here, which is subjected to a parabolic traction at the free end as shown in Fig. 5. The cantilever is assumed to have a uniform unit thickness so that plane stress condition is valid. The analytical solution is available and can be found in a textbook by Timoshenko and Goodier [28]:

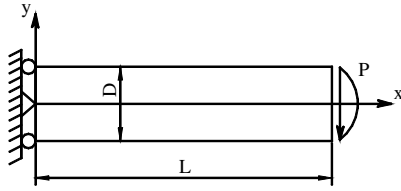


Fig. 5. Cantilever loaded at the end.

$$\begin{aligned} u_x &= \frac{Py}{6EI} \left[(6L - 3x)x + (2 + \nu) \left(y^2 - \frac{D^2}{4} \right) \right], \\ u_y &= -\frac{P}{6EI} \left[3\nu y^2(L - x) + (4 + 5\nu) \frac{D^2 x}{4} + (3L - x)x^2 \right], \end{aligned} \quad (37)$$

where the moment of inertia I for a beam with rectangular cross section and unit thickness is given by $I = \frac{D^3}{12}$.

The stresses corresponding to the displacements Eq. (37) are

$$\sigma_{xx}(x, y) = \frac{P(L - x)y}{I}; \quad \sigma_{yy}(x, y) = 0; \quad \tau_{xy}(x, y) = -\frac{P}{2I} \left(\frac{D^2}{4} - y^2 \right). \quad (38)$$

The related parameters are taken as $E = 3.0 \times 10^7$ kPa, $\nu = 0.3$, $D = 12$ m, $L = 48$ m and $P = 1000$ N. In the computations, the nodes on the left boundary are constrained using the exact displacements obtained from Eq. (37) and the loading on the right boundary uses the distributed parabolic shear stresses in Eq. (38).

The domain discretizations for three different elements: n -sided polygonal, quadrilateral and triangular elements are shown in Figs. 6–8, respectively. For the quadrilateral elements, to investigate the effect of the shape of the element when the severe distorted elements can be used, two types of discretization are used, as shown in Fig. 7: one with regular elements and the other with irregular interior nodes whose coordinates are generated in the following fashion:

$$\begin{aligned} x' &= x + \Delta x \cdot r_c \cdot \alpha_{ir}, \\ y' &= y + \Delta y \cdot r_c \cdot \alpha_{ir}, \end{aligned} \quad (39)$$

where Δx and Δy are initial regular element sizes in x - and y -directions, respectively. r_c is a computer-generated random number between -1.0 and 1.0 and α_{ir} is a prescribed irregularity factor whose value is chosen between 0.0 and 0.5 . The bigger the value of α_{ir} , the more irregular the shape of generated elements in the patch.

The numerical strain energies have been plotted against the number of nodes in Fig. 9. It can be seen that the NS-FEM, NS-FEM-Q4 and NS-FEM-T3 possess the upper bound property on the strain energy, i.e., the strain energies of NS-FEM, NS-FEM-Q4 and NS-FEM-T3 are always bigger than the exact one and converge to it with the increase of nodes. In the contrast, the SFEM, FEM-Q4 and FEM-T3 possess the lower bound property on the strain energy. These results imply a very simple procedure to

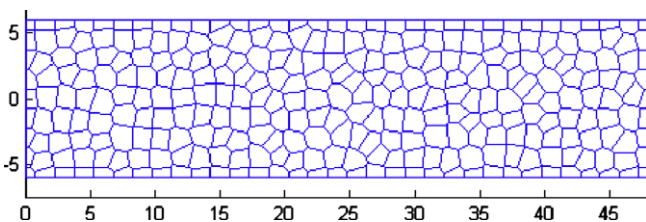


Fig. 6. Domain discretization of the cantilever using n -sided polygonal elements.

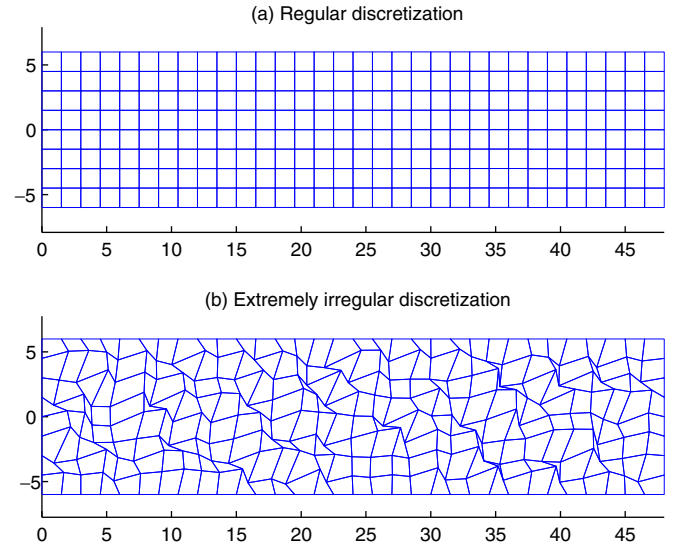


Fig. 7. Domain discretization of the cantilever using 4-node quadrilateral elements. (a) Regular elements; (b) extremely irregular elements ($\alpha_{ir} = 0.5$).

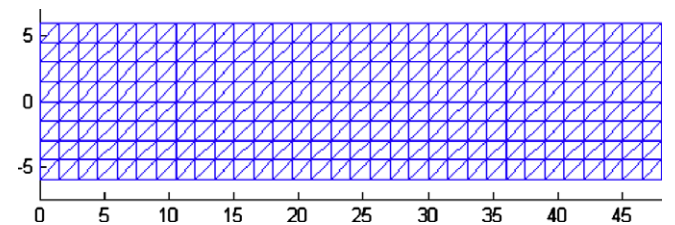


Fig. 8. Domain discretization of the cantilever using triangular elements.

determine an upper bound of the global error by using the NS-FEM together the SFEM or the FEM.

Fig. 10 shows the strain energy and the error norm in displacement against degree of nodal irregularity α_{ir} for the 4-node quadrilateral elements. The same analysis is still used but with distorted elements created by irregular nodes. The degree of nodal irregularity α_{ir} is chosen between 0.0 (regular mesh) and 0.5 . The results show that when the shape of element becomes distorted ($\alpha_{ir} = 0.1$ – 0.3), the accuracy of the FEM decreases gradually, while the accuracy of the NS-FEM still keeps stable. And when the shape of element is severe distorted ($\alpha_{ir} > 0.3$), the FEM fails to work due to the negative determinant of Jacobian matrix, while the NS-FEM still works well and stably.

7.2. Infinite plate with a circular hole

Fig. 11 represents a plate with a central circular hole of radius $a = 1$ m, subjected to a unidirectional tensile load of $\sigma = 1.0$ N/m² at infinity in the x -direction. Due to its symmetry, only the upper right quadrant of the plate is modeled. Plane strain condition is considered and $E = 1.0 \times 10^3$ N/m², $\nu = 0.3$. Symmetric conditions are imposed on the left and bottom edges, and the inner boundary of the hole is traction free. The exact solution for the stress is [28]

$$\begin{aligned} \sigma_{11} &= 1 - \frac{a^2}{r^2} \left[\frac{3}{2} \cos 2\theta + \cos 4\theta \right] + \frac{3a^4}{2r^4} \cos 4\theta, \\ \sigma_{22} &= -\frac{a^2}{r^2} \left[\frac{1}{2} \cos 2\theta - \cos 4\theta \right] - \frac{3a^4}{2r^4} \cos 4\theta, \\ \tau_{12} &= -\frac{a^2}{r^2} \left[\frac{1}{2} \sin 2\theta + \sin 4\theta \right] + \frac{3a^4}{2r^4} \sin 4\theta, \end{aligned} \quad (40)$$

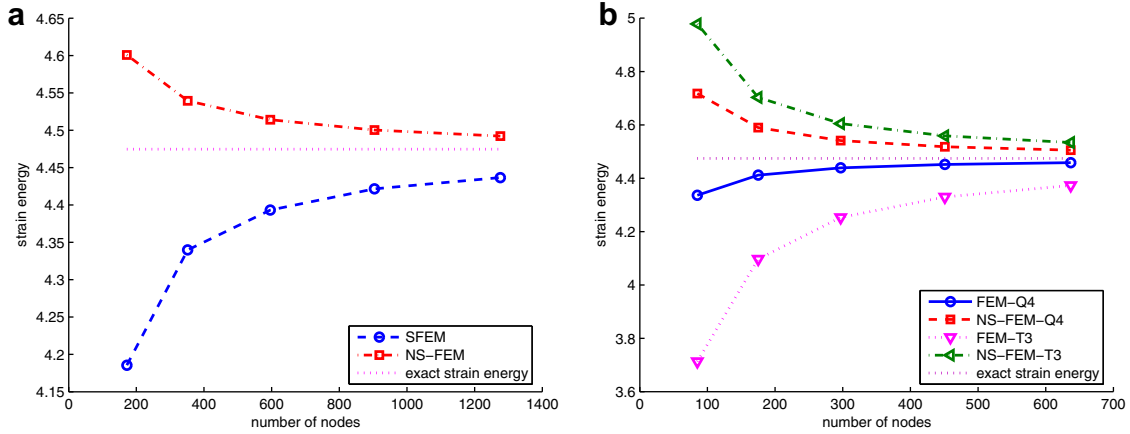


Fig. 9. Strain energy for the cantilever problem. (a) n -Sided polygonal elements; (b) triangular and 4-node elements.

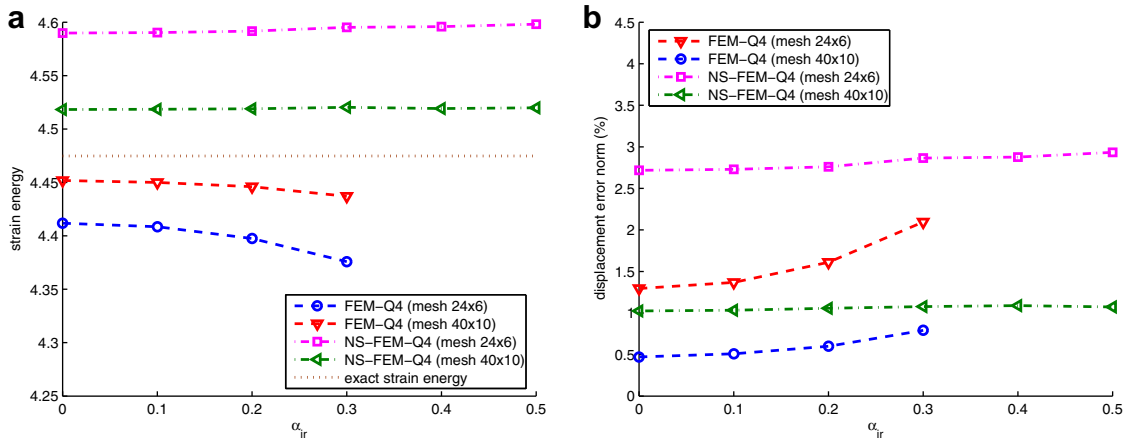


Fig. 10. (a) Strain energy; (b) displacement error norm of the cantilever problem using irregular meshes.

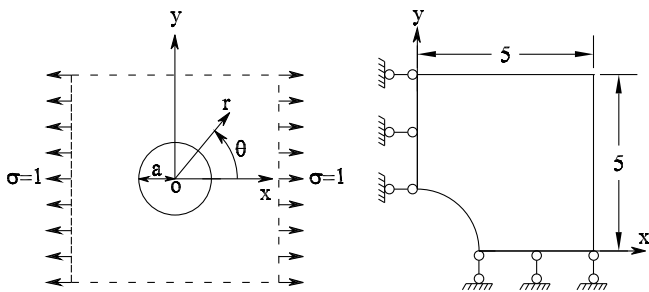


Fig. 11. Infinite plate with a circular hole and its quarter model.

where (r, θ) are the polar coordinates and θ is measured counter-clockwise from the positive x -axis. Traction boundary conditions are imposed on the right ($x = 5.0$) and top ($y = 5.0$) edges based on the exact solution Eq. (40). The displacement components corresponding to the stresses are

$$\begin{aligned} u_1 &= \frac{a}{8\mu} \left[\frac{r}{a} (\kappa + 1) \cos \theta + 2 \frac{a}{r} ((1 + \kappa) \cos \theta + \cos 3\theta) - 2 \frac{a^3}{r^3} \cos 3\theta \right], \\ u_2 &= \frac{a}{8\mu} \left[\frac{r}{a} (\kappa - 1) \sin \theta + 2 \frac{a}{r} ((1 - \kappa) \sin \theta + \sin 3\theta) - 2 \frac{a^3}{r^3} \sin 3\theta \right], \end{aligned} \quad (41)$$

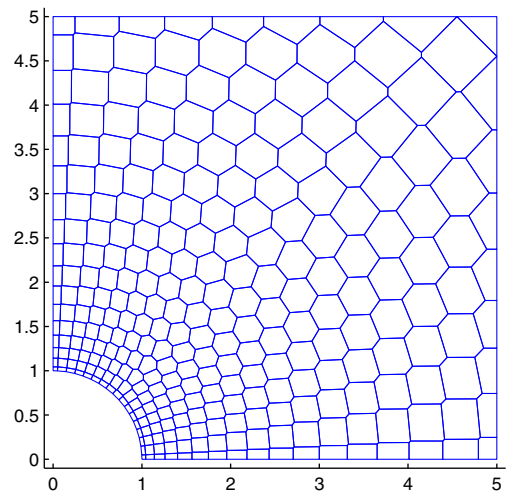


Fig. 12. Domain discretization of the infinite plate with a circular hole using n -sided polygonal elements.

where $\mu = E/(2(1 + \nu))$, κ is defined in terms of Poisson's ratio by $\kappa = 3 - 4\nu$ for plane strain cases.

Figs. 12 and 13 give the discretization of the domain using n -sided polygonal, 4-node quadrilateral and triangular elements, respectively.

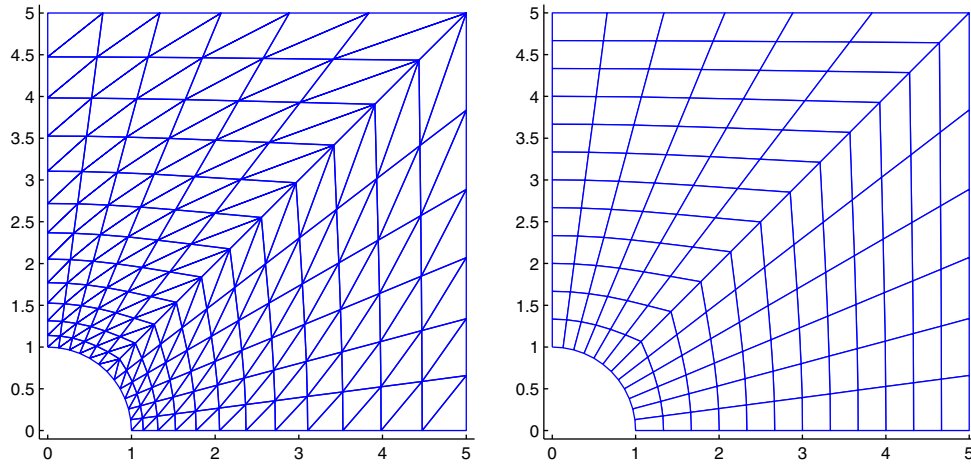


Fig. 13. Domain discretization of the infinite plate with a circular hole using triangular and 4-node quadrilateral elements.

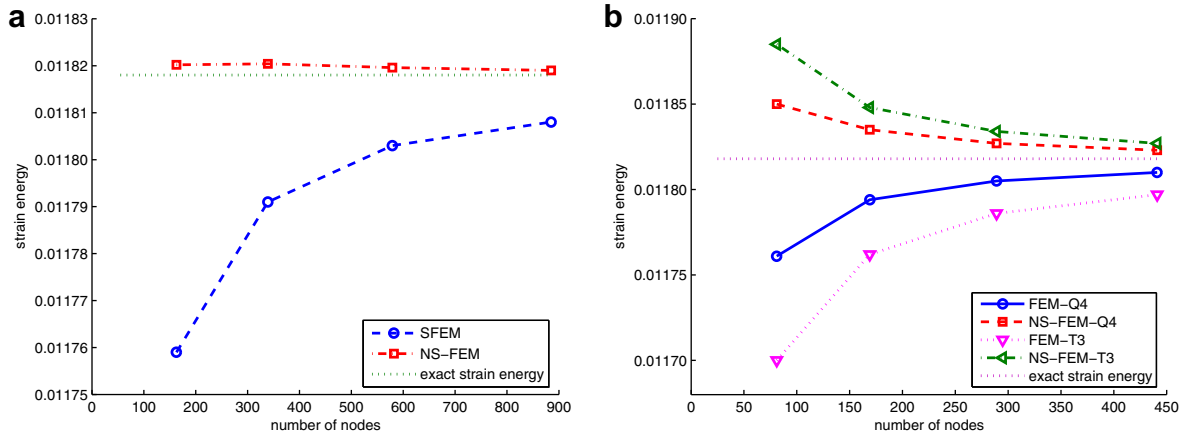


Fig. 14. Strain energy for the infinite plate with a circular hole. (a) n -Sided polygonal elements; (b) triangular and 4-node elements.

Fig. 14 again shows the upper bound property on the strain energy of the NS-FEM, NS-FEM-Q4 and NS-FEM-T3, while the SFEM, FEM-Q4 and FEM-T3 always keep the lower bound property.

From Figs. 15 and 16, it is observed that all the computed displacements and stresses of the NS-FEM using two discretizations with n -sided polygonal elements are in good agreement with the analytical solutions. With the refinement of the mesh, the accuracy is getting better.

Fig. 17 plots the displacement error norm versus different Poisson's ratios for n -sided polygonal elements (579 nodes) and for 4-node quadrilateral elements (mesh 16×16). The results show that the NS-FEM and NS-FEM-Q4 avoids the volumetric locking naturally, while the SFEM and FEM-Q4 are subjected to the volumetric locking. From this point, we have the next property of the NS-FEM:

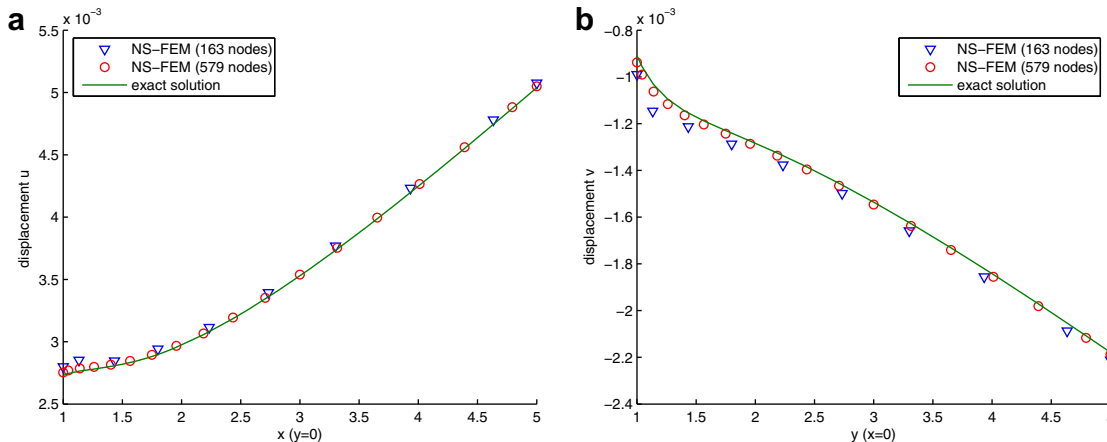


Fig. 15. Computed and exact displacements of the infinite plate with a circular hole. (a) Displacement u of nodes along bottom side; (b) displacement v of nodes along left side.

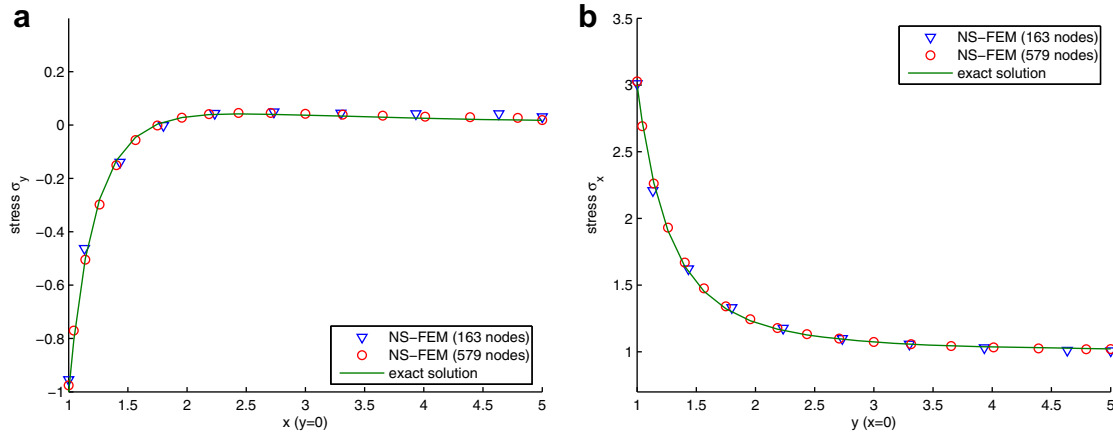


Fig. 16. Computed and exact stresses of the infinite plate with a circular hole. (a) Stress σ_y of nodes along bottom side; (b) stress σ_x of nodes along left side.

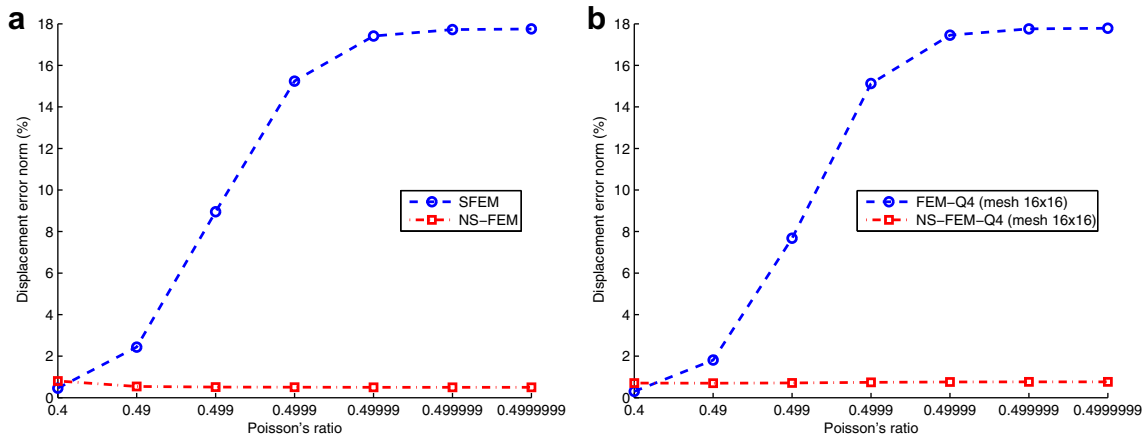


Fig. 17. Displacement error norm with different Poisson's ratios. (a) n -Sided polygonal elements (579 nodes); (b) 4-node quadrilateral elements.

Property 4. The NS-FEM is immune from the volumetric locking.

7.3. Semi-infinite plate

The semi-infinite plate shown in Fig. 18 is studied subjected to a uniform pressure within a finite range ($-a \leq x \leq a$). The plane strain condition is considered. The analytical stresses are given by [28]

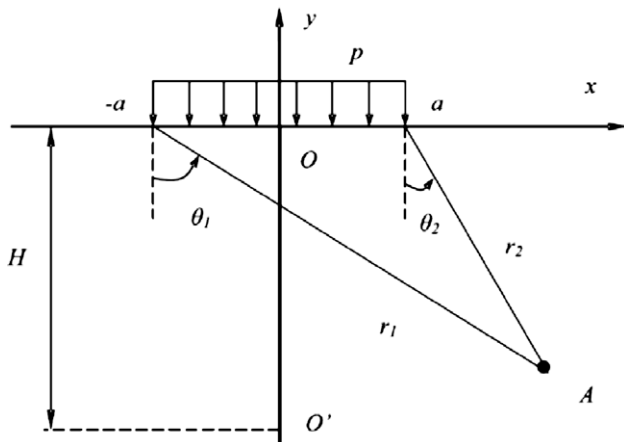


Fig. 18. Semi-infinite plate subjected to a uniform pressure.

$$\begin{aligned} \sigma_{11} &= \frac{p}{2\pi} [2(\theta_1 - \theta_2) - \sin 2\theta_1 + \sin 2\theta_2], \\ \sigma_{22} &= \frac{p}{2\pi} [2(\theta_1 - \theta_2) + \sin 2\theta_1 - \sin 2\theta_2], \\ \tau_{12} &= \frac{p}{2\pi} [\cos 2\theta_1 - \cos 2\theta_2]. \end{aligned} \quad (42)$$

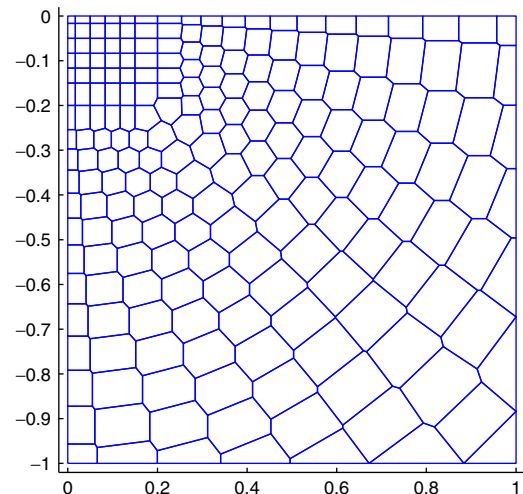


Fig. 19. Domain discretization of the semi-infinite plate using n -sided polygonal elements.

The directions of θ_1 and θ_2 are indicated in Fig. 18. The corresponding displacements can be expressed as

$$u_1 = \frac{p(1-\nu^2)}{\pi E} \left[\frac{1-2\nu}{1-\nu} [(x+a)\theta_1 - (x-a)\theta_2] + 2y \ln \frac{r_1}{r_2} \right],$$

$$u_2 = \frac{p(1-\nu^2)}{\pi E} \left[\frac{1-2\nu}{1-\nu} \left[y(\theta_1 - \theta_2) + 2H \arctan \frac{1}{c} \right] + 2(x-a) \ln r_2 - 2(x+a) \ln r_1 + 4a \ln a + 2a \ln(1+c^2) \right],$$
(43)

where $H=ca$ is the distance from the origin to point O' , the vertical displacement is assumed to be zero and c is a coefficient.

Due to the symmetry about the y -axis, the problem is modeled with a $5a \times 5a$ square with $a=0.2$ m, $c=100$ and $p=1$ MPa. The left and bottom sides are constrained using the exact displacements given by Eq. (43) while the right side is subjected to tractions computed from Eq. (42). Figs. 19 and 20 give the discret-

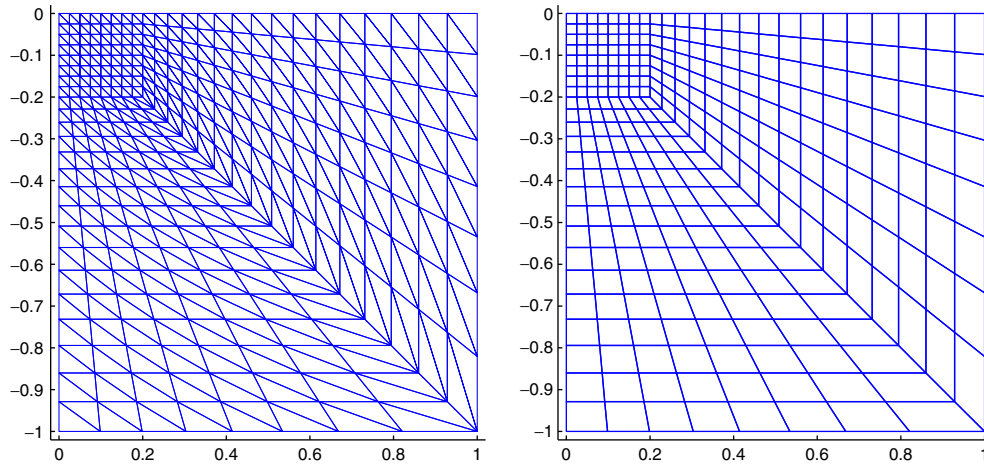


Fig. 20. Domain discretization of the semi-infinite plate using triangular and 4-node elements.

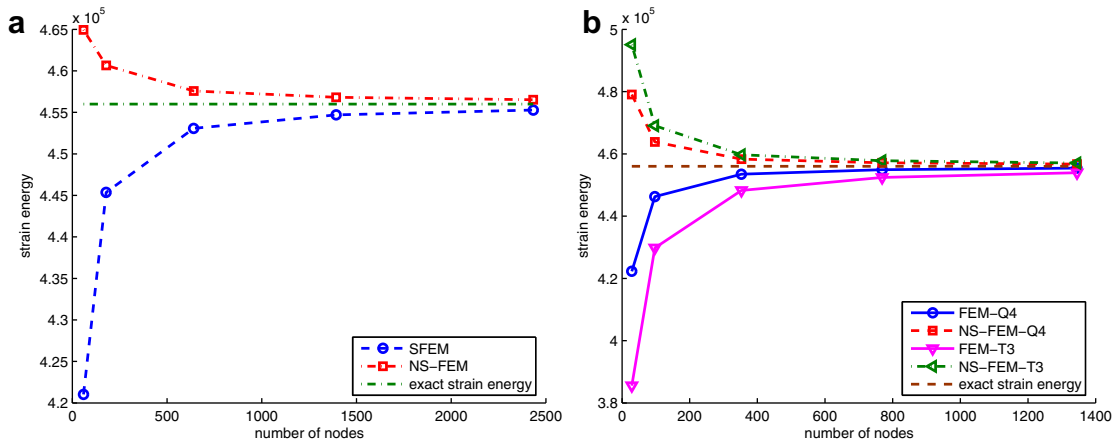


Fig. 21. Strain energy for the semi-infinite plate problem. (a) n -Sided polygonal elements; (b) triangular and 4-node elements.

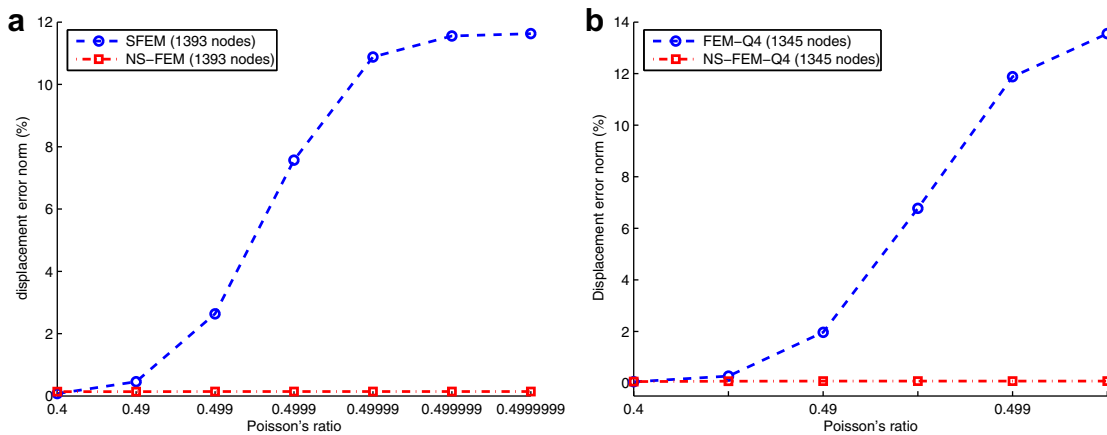


Fig. 22. Displacement error norm with different Poisson's ratios. (a) n -Sided polygonal elements; (b) 4-node quadrilateral elements.

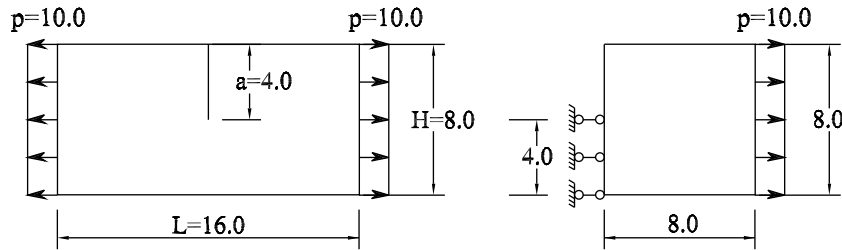


Fig. 23. Crack problem and half of the domain modeled.

ization of the domain using n -sided polygonal, 4-node quadrilateral and triangular elements, respectively.

Again, Fig. 21 shows the upper bound property on the strain energy of the NS-FEM, NS-FEM-Q4 and NS-FEM-T3, and the lower bound property of the SFEM, FEM-Q4 and FEM-T3. Fig. 22 verifies the immune property from the volumetric locking of the NS-FEM and NS-FEM-Q4.

7.4. Crack problem in linear elasticity

Consider a crack problem in linear elasticity as shown in Fig. 23. Data of the structure are $E = 1.0 \text{ N/m}^2$, $\nu = 0.3$, $t = 1 \text{ m}$. Due to the symmetry about the y -axis, only half of domain is modeled. One

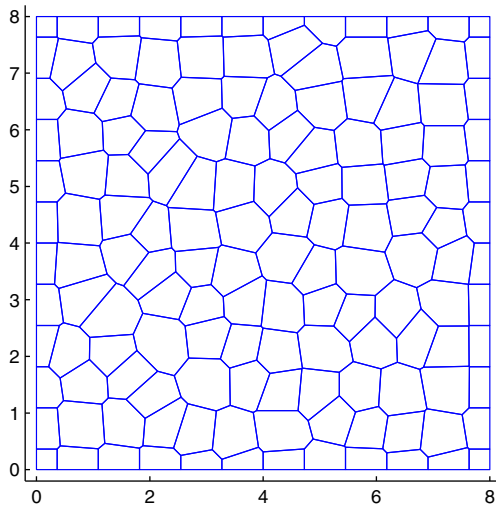


Fig. 24. Discretization of the crack problem using n -sided polygonal elements.

domain discretization using n -sided polygonal elements is shown in Fig. 24. By incorporating the dual analysis [13] and the procedure of Richardson's extrapolation with very fine meshes, Beckers et al. [29] proposed a good approximation of the exact strain energy to be 8085.7610.

Note that, the solution of the crack problem includes the strong singularity (namely a $r^{-1/2}$ in stress) at the crack tip. In the present study, we only estimate the results based on the global strain energy of entire domain. Hence discontinuity fields such as displacements and stresses along crack path should be further considered by incorporating the present method into the extended finite element method (XFEM) [30] which has been recently proved to be advantageous to solve crack problems.

Again, Fig. 25 confirms the upper bound property on the strain energy of the NS-FEM, NS-FEM-Q4 and NS-FEM-T3 and the lower bound property of the SFEM, FEM-Q4 and FEM-T3.

8. Conclusion

In this work, a node-based smoothed finite element method (NS-FEM) for upper bound solutions to solid mechanics problems is proposed. Through numerical results, some conclusions can be drawn as follows:

- The NS-FEM allows the use of polygonal elements with an arbitrary number of sides. The method can be applied easily to traditional 4-node quadrilateral or triangular elements without any modification.
- In the case of homogeneous essential boundary conditions, when a reasonably fine mesh is used, the NS-FEM possesses the upper bound property of the strain energy. A simple and practical procedure is proposed to determine both upper and lower bounds in the strain energy, by combining the NS-FEM with the SFEM (for n -sided polygonal elements) or with the FEM (for triangular or 4-node quadrilateral elements).

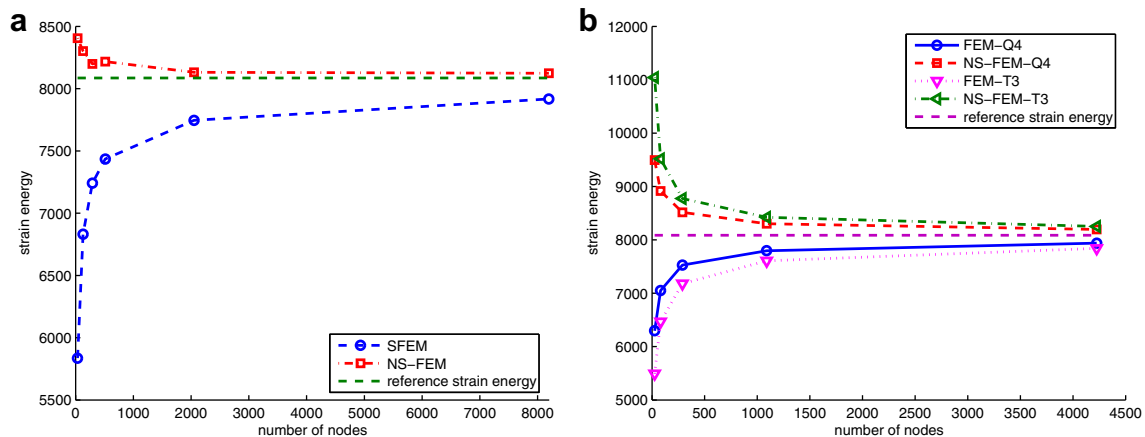


Fig. 25. Strain energy for the crack problem. (a) n -Sided polygonal elements; (b) triangular and 4-node elements.

- The NS-FEM is immune from the volumetric locking.
- In the NS-FEM, field gradients are computed directly only using shape functions themselves at some particular points along segments of boundary of the cells and no explicit analytical form is required. The values of shape functions for the discrete points of an n -sided polygonal element are defined in a trivial and simple manner.
- Unlike the conventional FEM using isoparametric elements, as no coordinate transformation or mapping is performed in the NS-FEM, no limitation is imposed on the shape of elements used herein. Even severely distorted elements are allowed. Domain discretization is more flexible than FEM.

References

- [1] Veubeke BF. Displacement and equilibrium models in the finite element method. In: Zienkiewicz OC, Holister GS, editors. Stress analysis. London: Wiley; 1965.
- [2] Ladeveze P, Coffignal G, Pelle JP. Accuracy of elastoplastic and dynamic analysis. In: Babuska I, Zienkiewicz OC, Gago J, Oliveira ER, editors. Accuracy estimates and adaptive refinements in finite element computations. New York: Wiley; 1986 [chapter 11].
- [3] Ladeveze P, Pelle JP, Rougeot P. Error estimation and mesh optimisation for classical finite elements. *Eng Comput* 1991;8:69–80.
- [4] Coorevits P, Ladeveze P, Pelle JP. An automatic procedure with a control of accuracy for finite element analysis in 2D elasticity. *Comput Methods Appl Mech Eng* 1995;121:91–121.
- [5] Almeida JPM, Freitas JAT. Alternative approach to the formulation of hybrid equilibrium finite elements. *Comput Struct* 1991;40:1043–7.
- [6] Pereira OJBA, Almeida JPM, Maunder EAW. Adaptive methods for hybrid equilibrium finite element models. *Comput Methods Appl Mech Eng* 1999;176:19–39.
- [7] Liu GR, Dai KY, Nguyen TT. A smoothed finite element method for mechanics problems. *Comput Mech* 2007;39:859–77.
- [8] Liu GR, Nguyen TT, Dai KY, Lam KY. Theoretical aspects of the smoothed finite element method (SFEM). *Int J Numer Methods Eng* 2007;71:902–30.
- [9] Liu GR, Nguyen-Thoi T, Lam KY. A novel alpha finite element method (α FEM) for exact solution to mechanics problems using triangular and tetrahedral elements. *Comput Methods Appl Mech Eng* 2008;197:3883–97.
- [10] Liu GR, Nguyen-Thoi T, Lam KY. A novel FEM by scaling the gradient of strains with factor α (α FEM). *Comput Mech* 2008; doi 10.1007/s00466-008-0311-1.
- [11] Liu GR, Zhang GY. Upper bound to elasticity problems: a unique property of the linearly conforming point interpolation method (LC-PIM). *Int J Numer Methods Eng* 2008;74:1128–61.
- [12] Almeida JPM, Pereira OJBA. Upper bounds of the error in local quantities using equilibrated and compatible finite element solutions for linear elastic problems. *Comput Methods Appl Mech Eng* 2006;195:279–96.
- [13] Debongnie JF, Zhong HG, Beckers P. Dual analysis with general boundary conditions. *Comput Methods Appl Mech Eng* 1995;122:183–92.
- [14] Chen JS, Wu CT, Yoon S, You Y. A stabilized conforming nodal integration for Galerkin meshfree method. *Int J Numer Methods Eng* 2000;50:435–66.
- [15] Yoo JW, Moran B, Chen JS. Stabilized conforming nodal integration in the natural-element method. *Int J Numer Methods Eng* 2004;60:861–90.
- [16] Liu GR, Zhang GY, Dai KY, Wang YY, Zhong ZH, Li GY, et al. A linearly conforming point interpolation method (LC-PIM) for 2D solid mechanics problems. *Int J Comput Methods* 2005;2(4):645–65.
- [17] Liu GR, Li Y, Dai KY, Luan MT, Xue W. A linearly conforming radial point interpolation method for solid mechanics problems. *Int J Comput Methods* 2006;3(4):401–28.
- [18] Dai KY, Liu GR, Nguyen TT. An n -sided polygonal smoothed finite element method (n SFEM) for solid mechanics. *Finite Elem Anal Des* 2007;43:847–60.
- [19] Dohrmann CR, Heinstein MW, Jung J, Key SW, Witkowski WR. Node-based uniform strain elements for three-node triangular and four-node tetrahedral meshes. *Int J Numer Methods Eng* 2000;47:1549–68.
- [20] Zhang GY, Liu GR, Wang YY, Huang HT, Zhong ZH, Li GY, et al. A linearly conforming point interpolation method (LC-PIM) for three-dimensional elasticity problems. *Int J Numer Methods Eng* 2007;72:1524–43.
- [21] Bathe KJ. Finite element procedures. Cambridge (MA), Englewood Cliffs (NJ): MIT Press; 1996.
- [22] Liu GR, Quek SS. The finite element method: a practical course. Oxford: Butterworth Heinemann; 2003.
- [23] Zienkiewicz OC, Taylor RL. The finite element method. 5th ed. Oxford: Butterworth Heinemann; 2000.
- [24] Pian THH, Wu CC. Hybrid and incompatible finite element methods. Boca Raton (FL): CRC Press; 2006.
- [25] Simo JC, Hughes TJR. On the variational foundations of assumed strain methods. *J Appl Mech* 1986;53:51–4.
- [26] Okabe A, Boots B, Sugihara K. Spatial tessellations: concepts and applications of Voronoi diagrams. Chichester: Wiley; 1992.
- [27] Liu GR. Meshfree methods: moving beyond the finite element method. Boca Raton, USA: CRC Press; 2002.
- [28] Timoshenko SP, Goodier JN. Theory of elasticity. 3rd ed. New York: McGraw-Hill; 1970.
- [29] Beckers P, Zhong HG, Maunder E. Numerical comparison of several a posteriori error estimators for 2D stress analysis. *Eur J Finite Elem Method* 1993;2(2).
- [30] Moës N, Dolbow J, Belytschko T. A finite element method for crack growth without remeshing. *Int J Numer Methods Eng* 1999;46:131–50.
- [31] Liu GR. A generalized gradient smoothing technique and the smoothed bilinear form for Galerkin formulation of a wide class of computational methods. *Int J Comput Methods* 2008;5(2):199–236.